Journal of Medicinal Chemistry

Article

pubs.acs.org/jmc

Glucocorticoid Receptor Modulators Informed by Crystallography Lead to a New Rationale for Receptor Selectivity, Function, and Implications for Structure-Based Design

Matthew W. Carson,[†] John G. Luz,[‡] Chen Suen,[†,§] Chahrzad Montrose,[†] Richard Zink,[†] Xiaoping Ruan,[†] Christine Cheng,[†] Harlan Cole,[†] Mary D. Adrian,[†] Dan T. Kohlman,[†] Thomas Mabry,[†] Nancy Snyder,[†] Brad Condon,[‡] Milan Maletic,[‡] David Clawson,[†] Anna Pustilnik,[‡] and Michael J. Coghlan*[,†]

[†]Lilly Research Laboratories, A Division of Eli Lilly & Co., Lilly Corporate Center, Indianapolis, Indiana 46285, United States

[‡]Eli Lilly Biotechnology Center, 10300 Campus Point Drive, Suite 200, San Diego, California 92121, United States

Supporting Information

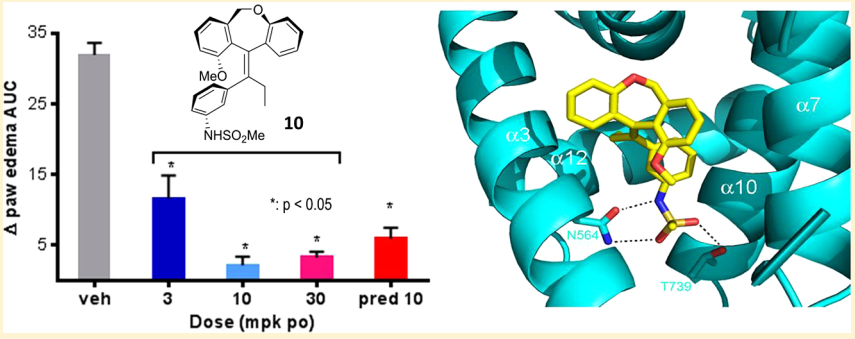

ABSTRACT: The structural basis of the pharmacology enabling the use of glucocorticoids as reliable treatments for inflammation and autoimmune diseases has been augmented with a new group of glucocorticoid receptor (GR) ligands. Compound **10**, the archetype of a new family of dibenzoxepane and dibenzosuberane sulfonamides, is a potent anti-inflammatory agent with selectivity for the GR versus other steroid receptors and a differentiated gene expression profile versus clinical glucocorticoids (lower GR transactivation with comparable transrepression). A stereospecific synthesis of this chiral molecule provides the unique topology needed for biological activity and structural biology. In vivo activity of **10** in acute and chronic models of inflammation is equivalent to prednisolone. The crystal structure of compound **10** within the GR ligand binding domain (LBD) unveils a novel binding conformation distinct from the classic model adopted by cognate ligands. The overall conformation of the GR LBD/**10** complex provides a new basis for binding, selectivity, and anti-inflammatory activity and a path for further insights into structure-based ligand design.

INTRODUCTION

Modulation of the glucocorticoid receptor (GR) has long been pursued as a favored target of medicinal and organic chemistry.[1,2] The discovery of cortisone and related steroidal GR modulators in the middle of the 20th century was followed by a decades-long effort prosecuting the steroid pharmacophore.[3] Ligands were sought that maintain anti-inflammatory efficacy, demonstrate selectivity versus related steroid hormone receptors, and reduce side effects associated with the endogenous function of glucocorticoids (GCs). New structural classes emerged, yet the goal of a novel functional GR ligand remained elusive until the 1990s when new chemotypes were discovered.[4,5] This was largely an empirical pursuit until the paradigm of differentiation of transrepression (TR) versus transactivation (TA) emerged.[6−8]

The GR mediates a breadth of biological processes (e.g., inflammation, gluconeogenesis, immunity, and homeostasis/development) through predominantly transcriptional mechanisms. The GR positively regulates transcription via TA, a process by which the GR, bound to an endogenous ligand, translocates from the cytoplasm into the nucleus where the resulting dimeric GR/ligand complex acts as an agonist and activates transcription by binding to glucocorticoid response elements (GREs) in susceptible promoter regions. The GR/ligand complex can also repress transcription, via the monomeric GR/ligand complex binding directly to transcription factors such AP-1 and NF-κB. The latter phenomenon is the prevailing mechanism of action for anti-inflammatory and immunosuppressant action.

Due to their potent anti-inflammatory properties, GR ligands have found broad application in the treatment of inflammation and autoimmune indications such as asthma, rheumatoid arthritis, and allergy. Clinically approved steroidal GR agonists

Received: October 18, 2013
Published: January 21, 2014

   dx.doi.org/10.1021/jm401616g | J. Med. Chem. 2014, 57, 849−860

include cortisol, prednisolone (pred), dexamethasone (dex), and fluticasone furoate. The side effects of steroidal GR agonists, attributed to GR-mediated TA, instigated research into the development of molecules that have an increased preference for GR-mediated TR. Such GR ligands are termed "dissociated" due to their discrimination between the pathways of TA (agonism) and TR. Maintenance of anti-inflammatory activity via TR of proinflammatory gene expression and reduction of side effects of endocrine function by attenuating agonism has been a preferred hypothesis for differentiation of GR pharmacology.[9−12] Yet, as the true complexity of GR-mediated processes has become apparent, it has been suggested that this hypothesis may be limited in its application as a paradigm for drug design.[13]

Selectivity has also been aggressively sought as cross reactivity with related steroid receptors the mineralocorticoid receptor (MR), the androgen receptor (AR), the progesterone receptor (PR), and the estrogen receptor (ER) would also potentiate dramatic physiological liabilities.[14] During these experiments, a clear structural basis for functional activity and selectivity has been the goal, yet the GR ligand binding domain (LBD) is among the most difficult of the steroid nuclear hormone receptors (NHRs) to crystallize. The first GR LBD crystal structure was disclosed using dex (Chart 1), and subsequently, the GR LBD binding conformations of more steroidal GR agonists and one steroid antagonist emerged.[15−17] The binding mode of a class of flexible trifluoromethyl carbinol GR agonists (TFCs), for example, GSK 866, (Chart 1)[16,18,19] was more recently described that occupies a novel channel originally observed in the crystal structure of A ring fused steroids such as deacyl cortivazol (Chart 1).[16,18−20] Novel GR ligands showing enhanced selectivity, differentiated function (TA vs TR), and oral in vivo activity have been disclosed, yet little structural information has emerged to influence ligand design.[9−12] We surmised that novel GR ligands could be identified with differentiated function based on a unique complex within the GR LBD. Herein, we characterize compound **10** with several close analogues that represent the first members of a novel class of potent, selective, and orally active GR ligands,[21−30] the crystal structure of compound **10** within the GR LBD, and the structural basis for TR activity and selectivity versus the remaining steroid NHRs.

Chart 1. Steroid and TFC GR Ligands

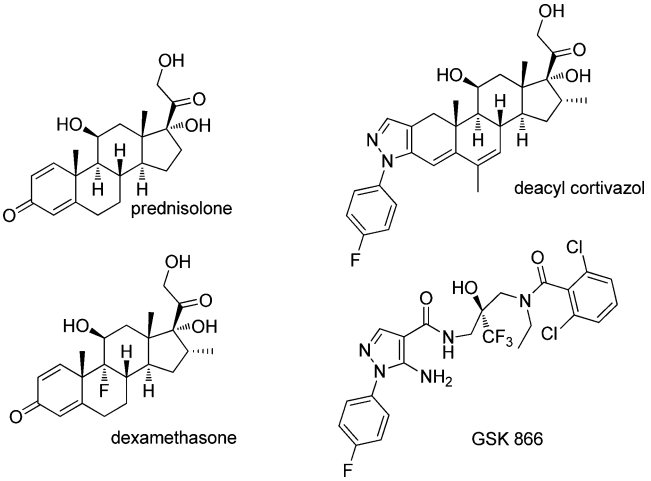

RESULTS

Scheme 1 details the synthesis of compound **10** that begins with the protection of 2-iodophenol (**1**) as its MOM ether (**2**)[31,32] followed by palladium-mediated Sonogashira coupling[33] with 1-butyne to provide acetylene **3**. Deprotection followed by Mitsunobu coupling[34] with 2-iodo-3-methoxybenzyl alcohol (**5**)[35] affords alkynyl ether **6** that was subjected to a recently reported[23] stereospecific sequence of platinum-catalyzed diboronation to intermediate **7** and cyclization to the dibenzoxepane vinyl boronate (**8**). The synthesis of **10** was completed by condensation of **8** with *N*-(3-iodophenyl) methanesulfonamide (**9**) to deliver this highly congested product in 13% overall yield for seven steps.

Notably, this molecule is intrinsically strained, since the coplanar substituents of the olefin must all adapt to the demanding steric environment by rotating out of conjugation with the double bond. The structural requirements of the tricylic system and the need to accommodate the benzylidene ring in close proximity to the methoxy substituent result in an overall molecular structure with a subtle and unusual element of planar chirality due to these steric interactions. The resulting increase in overall molecular volume is believed to be key to the successful realization of the GR LBD crystal structure versus several less strained members of this family (Chart 2). Although

Scheme 1. Preparation of Dibenzoxepane 10

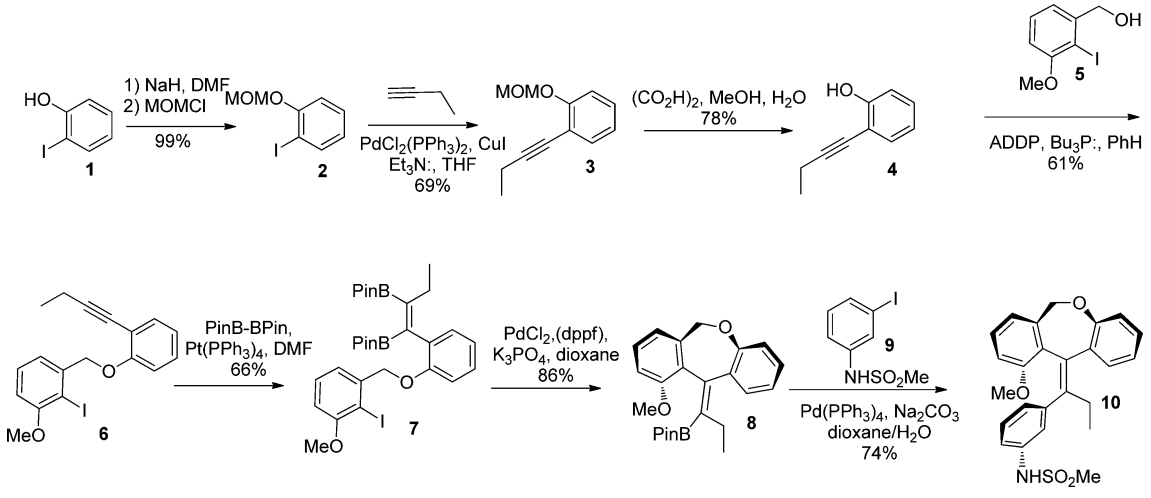

dx.doi.org/10.1021/jm401616g | J. Med. Chem. 2014, 57, 849−860

Chart 2. Depictions of Compound 10 within the GR LBD[a]

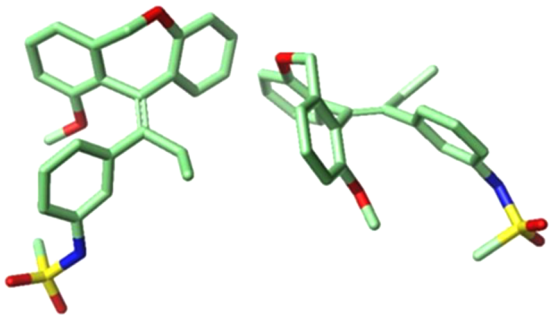

[a]Individual substituents of the double bond adapt to form a highly strained yet rigid three-dimensional structure to maintain coplanarity of the olefin substituents.

the synthesis implies no enantioselectivity, attempted separation of the enantiomers was unsuccessful using over 20 chiral solid phases under varied chromatographic conditions. Calculations of inversion barrier between enantiomers indicate a 70 kcal activation energy leading to the conclusion that interconversion of these rigid isomers under physiological conditions is unlikely.

Analogues **11**−**19** were prepared following published procedures.[23,26−28] These are less strained compounds where the substituents on the double bound are closer to coplanarity (**14** being an exception). Table 1 shows the binding data for members of this series as well as the commonly used GR clinical standards pred and dex. The structure−activity relationship (SAR) clearly indicates a preferred position on the benzylidene R_1 group for GR binding. The *meta*-substituted methylsulfonamides have attractive in vitro profiles in that they are potent (K_i < 1 nM) GR ligands with varying degrees of selectivity versus related steroid NHRs.

Comparison of the *m*-sulfonamides shows binding affinity of **10** for the GR is slightly better than pred with improved selectivity versus the MR. Binding affinity for the remaining steroid hormone receptors is also depicted in Table 1 where **10** shows a strong preference for the GR. In vitro functional assays were also performed for each of these receptors in agonist and antagonist modes versus relevant reference standards (Table S1, Supporting Information). In all cases, the functional activity seen for **10** is highly selective (>100×) compared to the other three potent GR ligands **11**−**13**. This molecule is also representative of differentiated function, since dibenzoxepane members of this series have lower maximal efficacy versus conventional glucocorticoids. Agonism of the GR is a measure of TA, and in this assay, **10** shows differentiated efficacy versus pred (53% for **10** versus 114% for pred at 10 μM, n = 10, see Chart S1, Supporting Information).

Compounds with binding K_i values less than 1 nM were tested in several TR models of anti-inflammatory activity. Of these, the IL-1β induced inhibition of IL-6 in CCD-39SK cells emerged as a strong indicator of in vivo efficacy.[36] Table 2 shows members of this family with potency comparable to pred in this assay.

Table 2. Inhibition of IL-1β Induced IL-6 in CCD-39SK Cells

compd	IC_{50} [nM], (SEM), n
10	4.38 (0.384) 11
11	4.80 (0.561) 5
12	9.32 (0.746) 4
13	75.9 (24.0) 7
pred	7.26 (0.276) 10

Several ensuing TR assays showed this sulfonamide to be equipotent and fully efficacious versus pred. For example, reduction of lipopolysaccharide (LPS)-induced TNFα in U937

Table 1. Comparison of NHR Binding for Dibenzosuberane and Dibenzoxepane Analogues

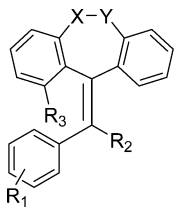

					binding K_i [nM][a]			
compd	R_1	R_2	R_3	X−Y	GR	AR	MR	PR
10	*m*-$NHSO_2Me$	Et	OMe	$-CH_2O-$	0.268 (0.026)	239 (51.0)	6.10 (4.58)	26.8 (6.33)
11	*m*-$NHSO_2Me$	Et	H	$-CH_2O-$	0.146 (0.053)2	9.74 (3.81)2	0.967 (0.176)2	15.5 (1.73)2
12	*m*-$NHSO_2Me$	Me	H	$-CH_2O-$	0.257 (0.041)	5.98	0.342 (0.0635)2	6.17
13	*m*-$NHSO_2Me$	H	H	$-CH_2CH_2-$	0.226 (0.054)	418 (150)	2.48 (1.79)	99.0 (40.7)
14	*m*-$N(Et)SO_2Me$	Et	OEt	$-CH_2O-$	>100	NT[b]	NT	NT
15	*o*-$NHSO_2Me$	H	H	$-CH_2CH_2-$	>100	NT	NT	NT
16	*p*-$NHSO_2Me$	H	H	$-CH_2CH_2-$	>100	NT	NT	NT
17	*m*-SO_2NHMe	H	H	$-CH_2CH_2-$	>100	NT	NT	NT
18	H	H	H	$-CH_2CH_2-$	>100	NT	NT	NT
19	*m*-NH_2	H	H	$-CH_2CH_2-$	>100	NT	NT	NT
pred					1.14 (0.295)	2520 (474)	0.290 (0.240)	>10 000
dex					0.690 (0.240)	1410 (706)	0.360 (0.160)	561 (196)

[a]All assays are the mean of n > 3 with each experiment run in triplicate unless indicated by a single value or n after the ± SEM shown in parentheses. [b]NT = not tested.

dx.doi.org/10.1021/jm401616g | J. Med. Chem. 2014, 57, 849−860

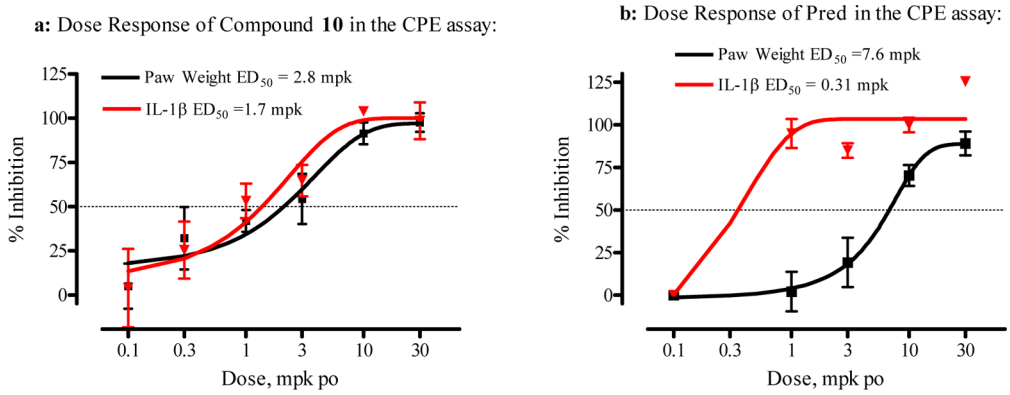

Figure 1. Acute evaluation of (a) compound **10** vs (b) prednisolone (pred) in the carrageenan-induced paw edema (CPE) assay. Compound **10** shows in vivo effects reducing paw weight (■) and IL-1β secretion (▼) comparable to that seen with pred.

cells[37,38] was comparable between these two ligands (compound **10** IC_{50} = 19.1 ± 9.3 nM (n = 3) vs IC_{50} = 8.2 ± 1.0 nM (n = 12) for pred). The overall profile of in vitro selectivity and TR activity led to compound **10** being selected for in vivo assessment.

Pharmacokinetics (PK) in the Sprague−Dawley rat summarized in Table S2 (Supporting Information) show an acceptable half-life ($t^1/_2$ = 1.4 h iv), high bioavailability (F = 100%), a low volume of distribution (V_d = 7 L/kg), and moderate clearance (56 mL/(min·kg)) suggestive of acceptable intravenous (iv) and oral (po) profiles. The relative equivalence in exposures in both the iv and po arms of this study (AUC = 1487 ± 562 and 1303 ± 108 (ng·h)/mL, respectively) supports both routes of administration, yet po dosing was used in subsequent in vivo assays.

In vitro characterization led to evaluation in in vivo models of anti-inflammatory activity. A pair of well-known assays, carrageenan-induced paw edema (CPE)[39] and collagen-induced arthritis (CIA),[40] were employed to assess the anti-inflammatory effects of **10**. Acute activity was measured in CPE where **10** shows improvements in overall inflammation as measured by changes in paw weight and inhibition of stimulated inflammatory cytokines such as IL-1β comparable to pred (Figure 1).

Evaluation of multidose efficacy in CIA was then assessed in therapeutic mode[41] where rats were dosed orally with pred and **10** for two weeks after disease onset. By using this model, compound **10** reduces signs and symptoms of disease on a time course comparable to pred (Figure 2a). Measures of overall change in paw edema by AUC, histological evaluation of bone resorption, pannus, cartilage damage, and joint inflammation show an improvement in **10**-treated groups. In many cases, the histology scores are superior to those seen in the pred-treated positive control group (Figure 2).

PK in the rat measured at the conclusion of the CIA live phase (day 15) is summarized in Table S2 (Supporting Information). Dose proportional exposures were observed with a T_{max} of 1 h and $t^1/_2$ values of 1.4−3.3 h depending on the dose. The overall profile is consistent with the earlier rat PK data at 3 mpk indicating no differences due to rat strain or the collagen adjuvant treatment (compare Tables S2 and S3, Supporting Information).

Although this sulfonamide demonstrates hormone receptor selectivity, TR activity, differentiated efficacy in GR agonist mode, and strong in vivo efficacy, an understanding of the fundamental binding mode of this nonsteroidal ligand within the GR LBD was lacking. The structural biology of glucocorticoids and related steroids is fairly well understood, yet the conformation of novel GR ligands within the GR LBD has not evolved to a level where their design assures receptor selectivity, anti-inflammatory function, and the potential to optimize druglike properties. To date, the GR LBD complexes of only two pharmacophores, steroids and trifluoromethyl carbinols (TFCs),[15,16,20,42] have emerged by way of X-ray crystallography, and in these cases, the argument has been made for ligands occupying a larger cavity leading to TR activity and a rationale for the limited NHR selectivity seen with these agents. We sought to define the corresponding binding interactions for these sulfonamides compared with known GR ligands beginning with steroidal reference standards.

The crystal structures of the GR LBD bound to dex as well as to other anti-inflammatory steroids reveal the key interaction of the steroid C-11 hydroxyl group with N564 of the GR LBD that is essential for TR activity. A similar role for the hydroxyl group of the TFCs is proposed based on subsequent structures of TFC/GR LBD complexes. In the case of steroids and TFCs, a hydroxyl group is employed to secure the key N564 interaction where additional β fluorine substitution can be used to attenuate the O−H bond strength and modulate TR potency.

We sought to crystallize this sulfonamide in complex within the GR LBD mindful of the need for N564 and the associated α helix 3 to adopt the proper conformation in active ligand complexes. Unlike other more planar analogues evaluated as candidates,[21,22] the unique topology of **10** imparted sufficient stability to the resulting complex to enable cocrystallization.

Structure of the GR LBD/Compound 10/D30 Complex. The overall crystal structure of compound **10** bound to the GR LBD (Figure 3, PDB accession code 4LSJ) is similar to that of previously determined cocrystal structures of GR LBD/agonist complexes (residues 522−777, F602Y, C638G) having an average rms deviation of 1.2 Å for all C_α atoms when superimposed upon the GR LBD dex bound structure (1M2Z),[15] excluding the α-1 helix (residues 559−777). The F602Y and C638G mutants enhance protein solubility to facilitate the GR LBD crystallization.[15] As had been observed in a previous GR LBD structures (3H52),[43] α helix 1 forms a domain swapping interaction, in this case with a symmetry related molecule (Figure S1, Supporting Information). Compound **10** is bound in the expected steroid ligand binding site found at the bottom of the domain and formed by generally

dx.doi.org/10.1021/jm401616g | J. Med. Chem. 2014, 57, 849−860

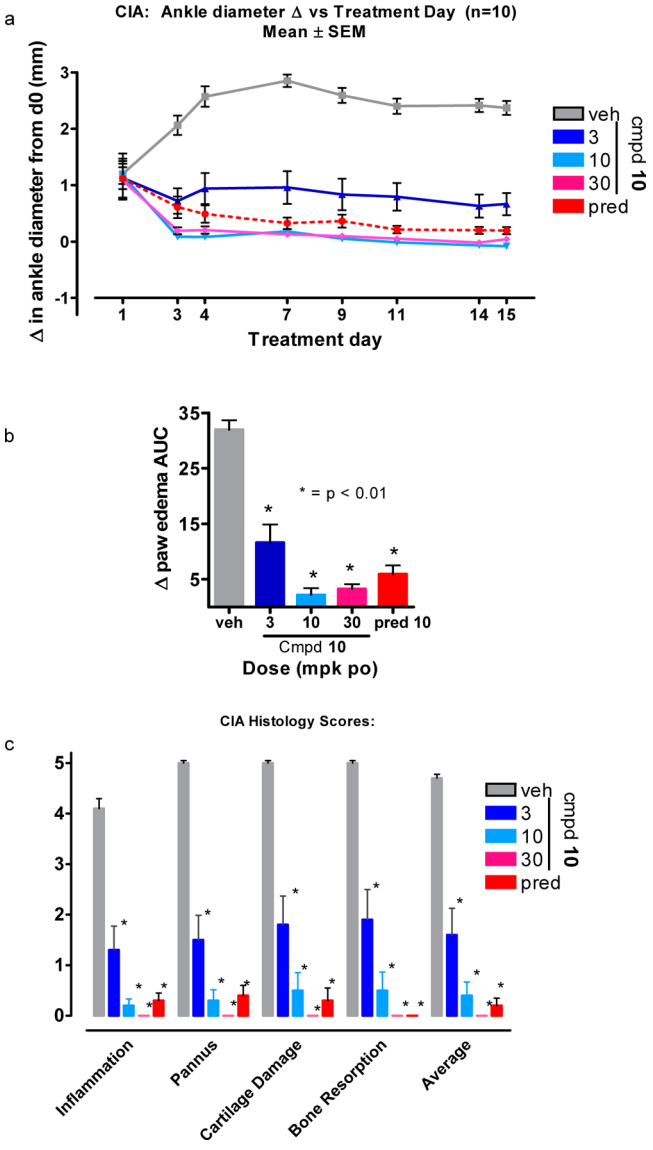

Figure 2. Data from the collagen-induced arthritis (CIA) model. Female Lewis rats were injected with collagen in the base of the tail, and disease was allowed to develop for 14 d. Groups (n = 10) of rats responding to the collagen challenge were selected and dosed daily with **10** or pred over the course of the following 15 d. (a) Changes in ankle diameter were measured throughout the study showing **10** dose dependently reduced inflammation with a time course comparable to a 10 mpk dose of pred (red dotted line). (b) AUC of paw diameter measures during live phase with statistical analysis. (c) Histology scores of the affected hindpaws. Scores: 5 = response equivalent to untreated collagen challenge group (vehicle control); 0 = response shows no histological changes versus normal healthy joint. Data indicate a strong response to **10** resulting in near normal joint histology at the highest test dose. *p values < 0.01 by Students t test versus the untreated vehicle control group.

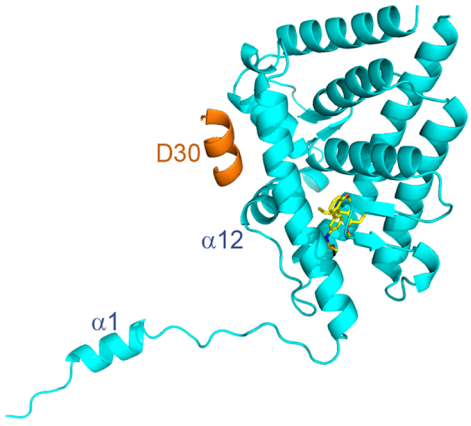

Figure 3. Structure of the GR LBD/D30/**10** trimeric complex (PDB accession 4LSJ). Ribbon diagram of the GR LBD (cyan) (residues 526−777) and the D30 peptide (orange) (residues 2−11) with **10** represented as sticks and colored by atom (C, yellow; N, blue; O, red). Compound **10** is bound in the steroid binding pocket with the methylsulfonamide pointing down.

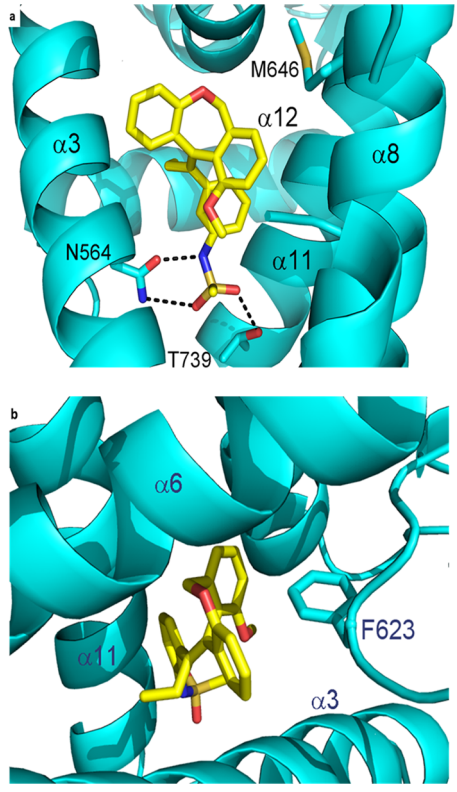

Figure 4. Comparison of GR (cyan) LBD/**10** crystal structure. (a) Methylsulfonamide of compound **10** (colored by atom) forms hydrogen bonds (2.5−3.5 Å) with the GR side chains of N546 and T739. H bonds are denoted by dotted lines. M646 is folded back. (b) The **10** tricycle interacts with the side chain of F623 through edge-to-face π-stacking with the two flanking aromatic rings of the dibenzoxepane.

hydrophobic residues contributed primarily by α helices 3, 6, 8, and 11 (Figure 3). (Helices are numbered according to the original estrogen receptor crystal structure.[44]) The cofactor mimic D30 peptide[45] is found in the coactivator binding site with the disposition of its LXXLL motif being in agreement with that of the canonical coactivator binding mode (see Figure S2, Supporting Information).

Compound **10** is oriented with the methylsulfonamide group α to the tricyclic ring structure (Figure 4a). The ligand/GR LBD side-chain contacts are entirely hydrophobic, with the exception being a pair of hydrogen bonds formed between the **10** methylsulfonamide and N564 of the GR LBD as well an another H bond with T739 (2.7, 3.1, and 2.6 Å respectively) (Figure 4a). The kinked tricyclic ring lies perpendicular to the long axis of the domain in the horizontal plane with its concave

dx.doi.org/10.1021/jm401616g | J. Med. Chem. 2014, 57, 849−860

surface facing the loop extending from the terminus of α helix 5. The two flanking aromatics and the central oxepane of the tricycle participate via the concave surface of **10**, in classic edge-to-face $\pi-\pi$ stacking interactions with the side chain phenyl of F623 (Figure 4b). The convex surface interacts with the side chains of M601, M604, and L732. The edge of the phenyl moiety of the tricycle interacts hydrophobically with L566 and is within hydrogen-bonding distance to the side-chain oxygen of Q570. Additional hydrophobic and van der Waals interactions are noted between the methoxyphenyl in **10** and the M639 and L563 side chains, and both carbons *ortho* to the sulfonamide nitrogen interact with the C736 and N564 side chains as well as the Y735 phenyl ring.[46]

Dibenzoxepane **10** and dex occupy roughly similar volumes within the steroid binding site and display comparable relative orientations. The steroid core of dex partially overlaps with the tricycle of **10**, and the dihydroxyacetyl group of the dex D ring points downward similar to the methylsulfonamide of **10** (Figure S4a, Supporting Information). The volume of the ligand in the GR LBD for **10** and dex bound structures are 311 and 300 Å^3, respectively. The A ring of dex lies nearly in the same plane as one of the phenyl rings in the tricycle of **10**; however, the B, C, and D rings of dex slope downward toward the bottom of the binding pocket as opposed to the tricycle of **10** that is enclosed within a region of hydrophobic side chains at the top of the LBD. The most significant deviation between the two binding modes occurs at the methoxyphenyl of **10** that projects outward toward α helix 8 into space occupied by the M646 side chain in the dex bound structure (compare Figures 4 and S4a, Supporting Information). The binding mode of **10** forces the rearrangement of the M646 side chain to accommodate the methoxyphenyl moiety, resulting in an upward shift of the M646 side chain by 6.4 Å. In addition, in the dex X-ray structure, a hydrogen bond is formed between the C-17 hydroxyl of the D ring and Q642 . In contrast, in the **10**-bound structure, the Q642 side chain folds back and in between α helices 8 and 11, a shift which is characterized by a 5.5 Å movement of the side-chain terminus. The only interaction between **10** and the Q642 side chain is via a long-range van der Waals contact (4.1 Å).

DISCUSSION

These GR ligands have been prepared by two general routes enabling a variey of analogues to be realized. Of these, the platinum-mediated pinacol diboronate route has been most reliable, especially when preparing sterically challenging analogues. The synthesis proceeds by a stereospecific route, yet for molecules such as **10** and **14**, there is no expectation of enantioselectivity. In the case of **10** and **14**, significant barriers to inteconversion are apparent, yet compounds lacking R_3 substituents adopt a planar orientation with lower steric concessions and a low barrier to interconversion. In vitro SAR from Table 1 indicates a clear preference for the *meta*-methysulfonamide containing an acidic proton capable of forming the required hydrogen bond with N564 (compare close analogues **10** and **14**). The added methoxy group in **10** versus **11**–**13** improves selectivity versus the MR, and the dibenzoxepanes emerge as partial agonists of the GR (compare **10**–**12** versus **13**, dex, and pred in Table S1, Supporting Information).

Dibenzoxepane **10** represents a novel ligand for the GR with differentiated TR versus TA function whose in vivo activity is similar to the reference steroid prednisolone. Compared to this reference, **10** shows strong activity in the acute CPE model of inflammation with respect to general anti-inflammatory response (reduction of paw weight) as well as measurement of specific cytokines (IL-1β). In a two week multidose study in an established model of rheumatoid arthritis (CIA) run in therapeutic mode, this dibenzoxepane has a comparable onset of action, overall efficacy, and improved protection of bone and joint degradation evaluated by histology. The overall PK profile is attractive, and notably, it is comparable across rat strains with no drastic effect from disease state. The overall in vivo efficacy is comparable to pred.

In addition to the in vitro and in vivo properties of **10** in vivo anti-inflammatory activity, receptor selectivity, and in vivo function, it provides a unique insight into structural requirements for GR ligands. Crystal structures of functional GR ligands in the LBD all have a hydrogen-bond interaction with N564 in helix 3 as a unifying trait associated with TR and anti-inflammatory activity. This mandatory interaction with N564 is maintained via the sulfonamide group of **10** acting not only as the noted hydrogen-bond donor but also as an acceptor resulting in a stronger association with the portion of the GR LBD needed for anti-inflammatory activity. The added hydrogen bond with T739 provides additional stabilization of the overall complex in the proper conformation.

With the key N564 interaction secure, the remainder of the dibenzoxepane binding mode digresses substantially from those seen with other chemotypes. In contrast to classic GR ligands, interactions associated with polar groups in the steroid D ring are absent for **10** that also does not form a "meta pocket" with a larger binding volume seen with TFCs and steroids. Compound **10** adopts a novel conformation involving interactions largely due to hydrophobic and van der Waals interactions resulting in a compact ligand/LBD complex similar to the endogenous ligand cortisol in terms of the overall volume, yet **10** is very different in its associated GR LBD residues.

Compound **10** does not interact with the canonical fashion with the trio of G/R/F residues found in all of the steroidal hormone receptors that are engaged by carbonyl or hydroxyl groups in the steroid A ring. In the GR/**10** complex, GR F623 now adopts an altered conformation through a novel edge to face interaction rather than the conventional $\pi-\pi$ face to face relationship seen for steroids thereby providing added stabilization of this unique complex. The binding conformation of **10** is much more distinct when compared to the TFCs (compare Figures 4a and S4b, Supporting Information). The TFC agonists (3E7C) take advantage of the plasticity of the GR binding pocket that had been noted in the deacylcortivazol crystal structure. A "meta" channel opens between α helices 3 and 6 allowing for the expansion of the steroid binding pocket, accommodating the deacylcortivazol phenylpyrazole extension of the steroid D ring. In contrast, **10** does not extend into any part of the "meta" channel nor does the TFC scaffold extend into the space occupied by the region containing the methoxyphenyl of the dibenzoxepane that thus far appears to be a unique aspect of **10** binding resulting in displacement of the M646 side chain. (Figure 5). As in the GR/dex crystal structure, the M646 side chain adopts an extended conformation in the GR/TFC complex that would not be compatible with **10** binding.

Many of the critical interactions between the GR and **10** appear to be potentially conserved in related NHRs. Among the GR, PR, MR, AR, and ERα, the phenylalanine that occupies

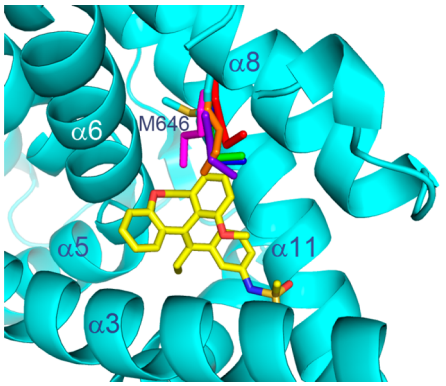

Figure 5. Methoxyphenyl of **10** occupies a unique space within the GR binding site. The crystal structure of GR LBD bound to **10** versus other GR LBD crystal structures comparing the side-chain positions of M646. The methoxyphenyl of **10** forces the M646 side chain to adopt a unique conformation. (The GR LBD is colored cyan with the **10** ligand colored by atom.) The color scheme for the methionine side chains in other GR LBD structures is as follows: dex, orange (1M2Z); TFC, magenta (3E7C); fluticasone furoate, green (3CLD); deacylcortivazol, purple (3BQD).

position 623 in the GR is structurally conserved (Figure 4b). The critical GR amino acids whose side-chain polar atoms interact with **10** are conserved in the PR and the MR (Figure 6).

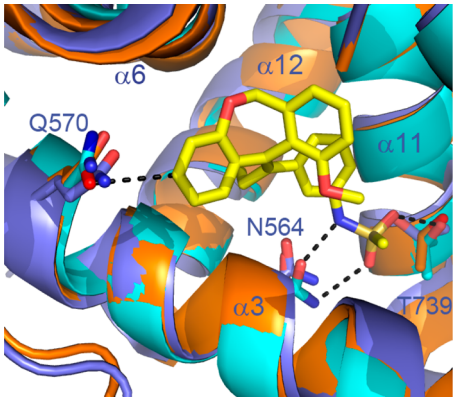

Figure 6. Critical binding interactions are conserved between the GR, PR, and MR. Crystal structures of the GR LBD (cyan), the PR (1ZUC) (orange), and the MR (2A3I) (slate blue) are superimposed and depicted as ribbon diagrams. Compound **10** and amino acid side chains are represented as sticks and colored by atom. Ligand interactions with polar atoms are represented by dashed lines. All polar side chain atoms that interact with **10** are preserved.

There is a structural basis for the observed steroid hormone selectivity. The hydrogen bond formed by the GR LBD T739 and **10** would not form in the AR or ERα as this threonine is replaced by leucine in both of these NHRs. Additionally, the critical N564 is replaced by a threonine in the ERα (Figure S5a, Supporting Information). The apparent conservation of critical binding features between the GR, PR, and MR prompts hypotheses about the cause of the noted selectivity of **10** toward the GR. This may be related to the freedom of rotation imparted to the M646 side chain by the presence of an alanine at position 605 in the GR. In the PR and AR, this position is occupied by valine that sterically prevents the extent of movement observed in the GR M646 side chain (Figure S5b,c, Supporting Information). No PR structure in the Protein Data Bank displays the equivalent methionine in the folded back conformation. However, in the MR/spironolactone crystal structure (3VHU), the equivalent methionine is found in the folded back position (Figure S5d, Supporting Information). The residue equivalent to GR A605 is MR S811 whose freedom of rotation may allow for the corresponding movement in the M852 side chain seen in the MR/spironolactone (antagonist) and the MR/aldosterone (agonist) crystal structure. One implication of this, if movement of M646 is important to GR binding and selectivity, is that the MR might be predicted to bind with higher affinity to **10** than would the PR. In fact, this is observed in binding studies (Table 1).

Selectivity versus other NHRs arises from subtle interactions associated with **10** and the resulting disposition of M646 and A605. By using this paradigm, it is possible to understand relative cross reactivity between NHRs informed by the interaction of these residues. The comparison of the MR and PR in this fashion led to a prediction of NHR selectivity supported by binding and functional data. The role of the methoxy group in the topology of **10** is a key factor in the binding configuration in that this group perturbed the overall structure of the ligand sufficiently to provide a stabilized complex within the LBD protein. The distinctive binding mode of this unique GR ligand suggests that leveraging the noted hydrophobic interactions associated with the novel F623 $\pi-\pi$ interactions, the disposition of M646 and A605 employed to provide receptor selectivity, and the mandated N564 interactions enable strategies for ligand design and reveal previously unexplored opportunities regarding functional requirements of the GR LBD and its associated ligands.

CONCLUSIONS

In summary, we have provided evidence for the in vitro and in vivo efficacy of a novel class of GR ligands. Key SAR features include the essential *meta*-sulfonamide on the benzylidene ring associated with TR and the observation that dibenzoxepanes provide partial agonist activity related with differentiated function. Of the molecules presented, compound **10** was selected for in vivo evaluation where it showed comparable efficacy and onset of action in acute and chronic anti-inflammatory models versus the clinical reference standard prednisolone. The unique topology of **10** enabled determination of the GR LBD/**10** binding mode that departs from canonical steroid binding interactions as well as those of recent GR ligands. The critical N564 hydrogen bond associated with anti-inflammatory activity is provided by the *meta*-sulfonamide thereby explaining the noted SAR trend. Moreover the remaining unusual interactions with F623 and side chains from the α8 helices contribute to the novel binding modes and the observed hormone receptor selectivity. The correlations between the in vitro and in vivo efficacy as well as the structural basis for many of the observed SAR trends in the context of the novel crystal structure provides guidance enabling the discovery of improved GR ligands.

EXPERIMENTAL SECTION

Materials and Methods. All reactions, unless specified, were carried out under an atmosphere of nitrogen in oven-dried glassware. Reagents and solvents were obtained from Aldrich Chemical, Acros Organics, or Strem and used without further purification. 1-Iodo-2-(methoxymethoxy)benzene (**2**) and (2-iodo-3-methoxy-phenyl)-methanol (**5**) were prepared according to the literature procedure

dx.doi.org/10.1021/jm401616g | J. Med. Chem. 2014, 57, 849−860

cited in the main paper. Thin layer chromatography was performed on 0.25 mm E. Merck silica gel 60 F254 plates and visualized under UV light. Flash chromatography was performed using Agilent Super Flash silica cartridges. Liquid chromatography−mass spectrometry (LC/MS) analysis was carried out on an Agilent 1100 Series LC/MSD using 5−100% acetonitrile/0.1% formic acid over 7.0 min. NMR spectra were recorded on a Varian 400, and chemical shifts are expressed in parts per million relative to solvent signals: $CDCl_3$ (^1H 7.26; ^{13}C 77.0 ppm) or DMSO-d_6 (^1H 2.50; ^{13}C 39.5 ppm). High-resolution mass spectra (HRMS) were obtained by electrospray (ESI) ionization. All compounds were refined to at least 95% purity via high-performance liquid chromatography.

*1-But-1-ynyl-2-(methoxymethoxy)benzene (**3**).* A solution of 1-iodo-2-(methoxymethoxy)benzene (**2**) (5.00 g, 18.9 mmol) in THF (100 mL) was degassed for 10 min with nitrogen in a 250 mL pressure flask prior to the addition of CuI (0.36 g, 1.9 mmol), $PdCl_2(PPh_3)_2$ (0.66 g, 0.95 mmol), and triethylamine (13.2 mL, 94.7 mmol). The resultant mixture was bubbled with nitrogen for 10 min and then with 1-butyne for 5 min; then, the flask was sealed, warmed to 50 °C, and stirred overnight. The mixture was partitioned between EtOAc (200 mL) and water (100 mL). The aqueous phase was extracted with EtOAc (100 mL). The combined organic phases were washed with brine (200 mL), dried over Na_2SO_4, and concentrated under reduced pressure to give a dark semisolid. Purification via flash chromatography (9:1 hexanes/EtOAc) gave 2.49 g (69%) of the titled compound as a tan oil: ^1H NMR (DMSO-d_6) δ 7.32 (dd, J = 8.0, 1.4 Hz, 1H), 7.23−7.27 (m, 1H), 7.10 (dd, J = 8.0, 1.4 Hz, 1H), 6.92 (td, J = 7.2, 1.2 Hz, 1H), 5.21 (s, 2H), 3.40 (s, 3H), 2.42 (q, J = 7.5 Hz, 2H), 1.14 (t, J = 7.5 Hz, 3H); ^{13}C NMR (DMSO-d_6) δ 157.7, 133.5, 129.5, 122.2, 115.9, 114.3, 96.0, 94.9, 76.6, 56.1, 14.3, 13.1.

*2-But-1-ynylphenol (**4**).* A solution of 1-but-1-ynyl-2-(methoxymethoxy)benzene (**3**) (2.49 g, 13.1 mmol) and oxalic acid (2.36 g, 26.2 mmol) in methanol (52 mL) and water (13 mL) was stirred at 55 °C for 3 days in a 500 mL round-bottomed flask. The reaction mixture was partially concentrated under reduced pressure. The aqueous mixture was extracted with diethyl ether (2 × 100 mL). The organic layers were combined, washed with brine (100 mL), dried over Na_2SO_4, and concentrated under reduced pressure. Purification via flash chromatography (9:1 hexanes/EtOAc) gave 1.49 g (78%) of the titled compound as a tan oil: ^1H NMR (DMSO-d_6) δ 9.62 (s, 1H), 7.20 (dd, J = 7.2, 1.4 Hz, 1H), 7.08−7.12 (m, 1H), 6.83 (dd, J = 8.0, 1.4 Hz, 1H), 6.71 (td, J = 7.2, 1.2 Hz, 1H), 2.39 (q, J = 7.6 Hz, 2H), 1.14 (t, J = 7.6 Hz, 3H); ^{13}C NMR (DMSO-d_6) δ 158.6, 133.3, 129.4, 119.3, 115.8, 111.1, 95.4, 77.2, 14.4, 13.1; HRMS (ESI) m/z calcd for $C_{10}H_{11}O$ $[M + H]^+$ = 147.0812, found 147.0804.

*1-[(2-But-1-ynylphenoxy)methyl]-2-iodo-3-methoxy-benzene (**6**).* Tri*n*-butylphosphine (4.0 g, 19 mmol) was added dropwise via syringe to a solution of 2-but-1-ynylphenol (**4**) (1.0 g, 6.8 mmol), 1-iodo-2-(methoxymethoxy)benzene (**5**) (1.7 g, 6.4 mmol) in benzene (32 mL) at 0 °C. ADDP (2.5 g, 9.7 mmol) was added in one portion to give a thick slurry that was allowed to warm to room temperature and then warmed to 50 °C for 18 h. The mixture was diluted with EtOAc (150 mL) and washed with 5 N NaOH (2 × 100 mL) and then brine (100 mL). The organic layer was dried over Na_2SO_4 and concentrated under reduced pressure. Purification via flash chromatography (95:5 hexanes/EtOAc) gave 1.53 g (61%) of the titled compound as a crystalline sold: ^1H NMR (DMSO-d_6) δ 7.19−7.38 (m, 4H), 6.90−7.01 (m, 3H), 6.71 (m, 1H), 5.08 (s, 2H), 3.78 (s, 3H), 2.42 (q, J = 7.6 Hz, 2H), 1.15 (t, J = 7.6 Hz, 3H); ^{13}C NMR (DMSO-d_6) δ 158.8, 158.1, 141.0, 133.4, 129.8, 129.7, 121.6, 121.0, 113.3, 113.5, 111.2, 96.4, 89.7, 76.7, 74.4, 57.0, 14.3, 13.1; HRMS (ESI) m/z calcd for $C_{18}H_{18}IO_2$ $[M + H]^+$ = 393.0353, found 393.0347.

*2-[(1Z)-1-[[2-[(2-Iodo-3-methoxy-phenyl)methoxy]phenyl]-(4,4,5,5-tetramethyl-1,3,2-dioxaborolan-2-yl)methylene]propyl]-4,4,5,5-tetramethyl-1,3,2-dioxaborolane (**7**).* A 75 mL screw-top vessel was charged with 1-[(2-but-1-ynylphenoxy)methyl]-2-iodo-3-methoxy-benzene (**6**) (1.44 g, 3.67 mmol) and DMF (30 mL), and the solution was purged with nitrogen for 15 min. Bis(pinacolato)diboron (1.28 g, 4.77 mmol) was added in a single portion followed by $Pt(PPh_3)_4$ (0.461 g, 0.367 mmol), and the mixture was heated at 80 °C for 18 h. The reaction was allowed to cool to room temperature and partitioned between EtOAc (100 mL) and water (50 mL). The layers were separated, and the aqueous layer was extracted with EtOAc (50 mL). The combined organic layers were washed with water (5 × 50 mL) and then brine (50 mL). The organic layer was dried with Na_2SO_4, filtered, and concentrated under reduced pressure. Purification via flash chromatography (95:5 hexanes/EtOAc) gave 1.56 g (66%) of the titled compound as an off-white powder: ^1H NMR (DMSO-d_6) δ 7.25 (t, J = 8.0 Hz, 1H), 7.09−7.14 (m, 1H), 7.04 (d, J = 6.8 Hz, 1H), 6.88−6.92 (m, 3 H), 6.72 (d, J = 8.0 Hz, 1H), 4.97 (s, 2H), 3.83 (s, 3H), 1.95 (q, J = 7.6 Hz, 2H), 1.28 (s, 12 H), 1.10 (s, 12H), 0.85 (t, J = 7.6 Hz, 3H); ^{13}C NMR (DMSO-d_6) δ 157.4, 154.6, 140.6, 131.0, 129.4, 129.0, 127.4, 120.6, 120.2, 112.3, 110.4, 88.0, 83.1 (2C), 73.9, 56.5, 39.7−40.1 (m, 2C), 24.6−26.9 (m, 4C); HRMS (ESI) m/z calcd for $C_{30}H_{43}B_2IO_7$ $[M + H_2O]^+$ = 664.2288, found 664.2481.

*2-[(1E)-1-(10-Methoxy-6H-benzo[c][2]benzoxepin-11-ylidene)-propyl]-4,4,5,5-tetramethyl-1,3,2-dioxaborolane (**8**).* A 150 mL screw-top vessel was charged with **6** (0.39 g, 0.99 mmol) and dioxane (93 mL), and the solution was purged with nitrogen for 15 min. Potassium phosphate (0.76 g, 3.5 mmol) was added in a single portion followed by $PdCl_2$dppf·CH_2Cl_2 (0.097 g, 0.12 mmol), and the mixture was heated at 80 °C for 18 h. The reaction was allowed to cool to room temperature and partitioned between EtOAc (150 mL) and water (100 mL). The layers were separated, and the aqueous layer was extracted with EtOAc (50 mL). The combined organic layers were washed with water (5 × 50 mL) and then brine (50 mL). The organic layer was dried with Na_2SO_4, filtered, and concentrated under reduced pressure. Purification via flash chromatography (95:5 hexanes/EtOAc) gave 0.39 g (86%) of the titled compound as an off-white powder: ^1H NMR (DMSO-d_6) δ 7.19 (dd, J = 8.4, 7.6 Hz, 1H), 7.07−7.11 (m, 1H), 6.90−7.00 (m, 2H), 6.91 (dd, J = 8.0, 0.8 Hz, 1H), 6.80 (td, J = 8.0, 1.2 Hz, 1 H), 6.67 (td, J = 8.0, 1.2 Hz, 1 H), 5.52 (d, J = 12.0 Hz, 1H), 4.80 (d, J = 12.0 Hz, 1H), 3.66 (s, 3H), 2.22−2.31 (m, 2 H), 1.03 (s, 6H), 0.96 (s, 6H), 0.94 (t, J = 7.2 Hz, 3H); ^{13}C NMR (THF-d_5) δ 155.0, 154.8, 141.6, 136.7 (br, low intensity olefin C binding to B), 134.8, 133.6, 130.6, 128.4, 127.1, 125.4, 119.7, 118.9 (2C), 111.1, 82.3, 69.1, 54.8, 24.7, 23.8, 14.0; HRMS (ESI) m/z calcd for $C_{24}H_{31}BO_4$ $[M + H]^+$ = 393.2355, found 393.2348.

*N-[3-[(1Z)-1-(10-Methoxy-6H-benzo[c][1]benzoxepin-11-ylidene)propyl]phenyl] methanesulfonamide (**10**).* A 50 mL microwave vial was charged with **7** (0.16 g, 0.41 mmol), *N*-(3-iodophenyl)methanesulfonamide (**9**) (0.19 g, 0.61 mmol), 3,5-dimethoxyphenol (0.32 g, 2.0 mmol), potassium hydroxide (0.40 g, 6.1 mmol), water (1.6 mL), and dioxane (4.1 mL), and the solution was purged with nitrogen for 15 min. $Pd(PPh_3)_4$ (0.047 g, 0.041 mmol) was added in a single portion, the reaction vessel was sealed, and the mixture was heated at 80 °C for 18 h. The reaction was allowed to cool to room temperature and partitioned between EtOAc (50 mL) and 5 N sodium hydroxide (20 mL). The layers were separated, and the organic layer was washed with water (30 mL) and then brine (30 mL). The organic layer was dried with Na_2SO_4, filtered, and concentrated under reduced pressure. Purification via flash chromatography (4:1 hexanes/EtOAc) gave 131 mg (74%) of the titled compound as a clear crystalline solid: ^1H NMR (DMSO-d_6) δ 9.43 (s, 1H), 7.19 (dd, J = 8.0, 0.4 Hz, 1H), 7.04−7.15 (m, 3H), 6.91 (dd, J = 9.2, 0.8 Hz, 1H), 6.84−6.92 (m, 3H), 6.75−6.77 (m, 1H), 6.80 (dd, J = 8.0, 1.2 Hz, 1 H), 6.67 (d, J = 7.6, 1 H), 5.74 (d, J = 12.0 Hz, 1H), 4.94 (d, J = 12.0 Hz, 1H), 3.30 (s, 3H), 2.76−2.85 (m, 2H), 2.60 (s, 3H), (s, 3 H), 0.79 (t, J = 7.4 Hz, 3H); ^{13}C NMR (DMSO-d_6) δ 156.9, 155.9, 145.0, 143.6, 139.5, 136.1, 134.6, 133.3, 131.0, 130.4, 129.6, 129.4, 126.7, 125.7, 121.8, 121.5, 121.0, 120.7, 119.4, 113.0, 71.3, 56.2, 39.6, 28.6, 14.3; HRMS (ESI) m/z calcd for $C_{25}H_{26}NO_4S$ $[M + H]^+$ = 436.1584, found 436.1576.

The chemistry described above as well as previously reported procedures[26−28] affords the following products:

*N-[3-[(1Z)-1-(10-Ethoxy-6H-benzo[c][1]benzoxepin-11-ylidene)-propyl]phenyl]-N-ethyl-methanesulfonamide (**14**).* ^1H NMR (400 MHz, DMSO-d_6): δ (ppm) 0.70 (t, J = 7.2 Hz, 3H), 0.79 (t, J = 7.25 Hz, 3H), 1.13 (t, J = 7.0 Hz, 3H), 2.50−2.62 (m, 1H), 2.72 (s, 3H),

dx.doi.org/10.1021/jm401616g | J. Med. Chem. 2014, 57, 849−860

2.76−2.88 (m, 1H), 3.25−3.38 (m, 2H), 3.38−3.50 (m, 1H), 3.66−3.77 (m, 1H), 4.94 (d, J = 12 Hz, 1H), 5.80 (d, J = 12 Hz, 1H), 6.63 (d, J = 8.13 Hz, 1H), 6.73 (dd, J = 8.24/1.21 Hz, 1H), 6.78−6.82 (m, 1H), 6.87 (dt, J = 7.06/1.21 Hz, 1H), 6.95 (d, J = 7.03 Hz, 1H), 7.03−7.16 (m, 4H), 7.16−7.20 (m, 1H), 7.20−7.26 (m, 1H). MS $[M + H]^+$ calcd: 477.6, found: 477.8; $[M + Na]^+$ found: 499.6.

*N-(2-((10,11-Dihydro-5H-dibenzo[a,d][7]annulen-5-ylidene)-methyl)phenyl)methanesulfonamide (**15**).* ^{1}H NMR (400 MHz, DMSO-d_6): δ (ppm) 2.80−3.04 (m, 2H), 3.07 (s, 3H), 3.28−3.48 (m, 2H), 6.64 (dd, J = 1.5, 7.9 Hz, 1H), 6.87−6.95 (m, 3H), 7.00 (s, 1H), 7.11−7.16 (m, 3H), 7.20−7.25 (m, 2H), 7.28 (dd, J = 1.0, 8.0 Hz, 2H), 7.60−7.62 (m, 1H), 9.39 (1H, bs). MS $[M + H]^+$ calcd: 376.49, found: 375.8; $[M + Na]^+$ found 397.8.

*N-(4-((10,11-Dihydro-5H-dibenzo[a,d][7]annulen-5-ylidene)-methyl)phenyl)methanesulfonamide (**16**).* ^{1}H NMR (400 MHz, DMSO-d_6): δ (ppm) 2.80−2.97 (m, 2H), 2.94 (s, 3H), 2.25−2.40 (m, 2H), 6.72 (s, 1H), 6.90−6.95 (m, 1H), 6.94 (s, 4H), 7.03−7.11 (m, 2H), 7.17−7.20 (m, 2H), 7.23 (dt, J = 7.8/1.2 Hz, 1H), 7.34 (dd, J = 7.5/1.1 Hz, 1H), 7.44 (dd, J = 5.8/3.4 Hz, 1H), 9.70 (s, 1H). MS $[M + H]^+$ calcd: 376.49, found: 397.80 $[M + Na]^+$.

*5-Benzylidene-10,11-dihydro-5H-dibenzo[a,d][7]annulene (**18**).* ^{1}H NMR (400 MHz, DMSO-d_6): δ (ppm) 2.78−3.00 (m, 2H), 3.24−3.46 (m, 2H), 6.81 (s, 1H), 6.88 (dd, J = 7.5/1.2 Hz, 1H), 6.98−7.05 (m, 3H), 7.06−7.16 (m, 4H), 7.18−7.24 (m, 3H), 7.34 (dd, J = 7.5/1.2 Hz, 1H), 7.46 (dd, J = 5.7/3.3 Hz, 1H). MS $[M - H]^-$ calcd: 281.38, found: 280.80 $[M - 1]^-$.

Compounds **11**, **12**, **13**, **17**, and **19** have been previously characterized.[26−28]

Binding Assays. Cell lysates from human embryonic kidney HEK293 cells overexpressing human MR, GR, AR, ER, or PR and ^{3}H-aldosterone for the MR, ^{3}H-dexamethasone for the GR, ^{3}H-estradiol for the ER, and ^{3}H-methyltrienolone for the AR and PR are used for receptor−ligand competition binding assays to determine K_i values. Competing test compounds are added from 0.01 nM to 10 μM. The data are used to calculate an estimated IC_{50} and percentage inhibition at 10 μM. The IC_{50} values for compounds are converted to K_i using the Cheng−Prushoff equation. Values shown are the mean values of at least three experiments each run in triplicate.

In Vitro Functional Assays (Agonist/Antagonist). Human embryonic kidney HEK 293 cells were transfected with receptors and reporter gene plasmids. The reporter plasmid containing two copies of probasin ARE (androgen response element 5′-GGTTCTTGGAG-TACT-3′) and the TK promoter upstream of the luciferase reporter cDNA was transfected with a plasmid constitutively expressing hAR using the viral CMV promoter. The reporter plasmid containing two copies of GRE (glucocorticoid response element 5′-TGTACAG-GATGTTCT-3′) and the TK promoter upstream of the luciferase reporter cDNA was transfected with a plasmid constitutively expressing either hGR, hMR, or hPR, using the viral CMV promoter. Cells were transfected in DMEM media with 5% charcoal-stripped fetal bovine serum (FBS). After an overnight incubation, cells were trypsinized, plated in 96 well plates, incubated for 4h, and then exposed, to 0.01 nM to 10 μM of test compounds in half log dilutions. In the antagonist assays, low concentrations of agonist for each respective receptor are added to the media (0.25 nM dexamethasone for the GR, 0.3 nM methyltrienolone for the AR, 0.05 nM promegestrone or R5020 for the PR, and 0.05 nM aldosterone for the MR). After 24 h incubation with the compounds, cells are lysed, and the luciferase activity is determined. Data are fitted to a four parameter-fit logistics to determine EC_{50} values. The percentage efficacy is determined versus maximum stimulation obtained with 100 nM methyltrienolone for the AR assay, with 30 nM promegestrone for the PR assay, 30 nM aldosterone for the MR assay, and 100 nM dexamethasone for the GR assay.

TR Assays. *Il-1β Stimulated IL-6 in CCD-39SK Cells.* CCD-39SK cells were seeded onto 96-well cell culture plates at 20 000 cells/well in modified Eagle MEM media containing 2% charcoal/dextran-treated FBS and incubated at 37 °C in a 5% CO_2 incubator. Compound diluents in 96-well master plate were used with dexamethasone at 0.4 μM and 0.4% DMSO as positive and negative controls, respectively. The cells were pretreated with compounds (50 μL/well of 4X stock) for 60 min. Finally, rhIL-1β at a final concentration of 1 ng/mL was added. The cells were incubated at 37 °C in a CO_2 incubator for 24 h. A 100 μL amount of culture supernatant was transferred from each well to the 96 wells and spun at 2000 rpm for 10 min at 4 °C in an Eppendorf 5810R centrifuge to remove the cells. The flowthrough was used directly for IL-6/cytokine/chemokine measurement. Each compound was evaluated using 10 point half log dilutions with each concentration representing the mean of triplicate assessment.

LPS-Stimulated TNFα in PMA-Differentiated U-937 Cells. U-937 cells were seeded onto 96-well cell culture plates at 100 000 cells/well, 200 μL/well of 20 nM PMA in media was added, and the cells were incubated overnight (∼24 h) at 37 °C in a 5% CO_2 incubator. The medium was removed, and the cells were refed 200 μL/well of media without PMA . The cells were treated with compounds (50 μL/well of 4X stock) for 60 min. LPS (50 μL/well of 400 ng/mL stock) was then added, and the cells were incubated at 37 °C in a 5% CO_2 incubator for 24 h. Secreted TNFα was then measured using 25 μL/well of filtrate via EIA/RIA and quantified. Each compound was evaluated using 10 point half log dilutions with each concentration representing the mean of triplicate assessment.

In Vivo Assays. *Pharmacokinetics.* Cannulated male Sprague−Dawley rats were fasted overnight prior to receiving 3 mpk doses of compound **10** at t = 0. (iv formulation: 20% microemulsion, 80% DI water; po formulation: CMC/tween in DI water) Approximately 0.2 mL of blood was collected via cannula in heparin-coated collection tubes at t = .08, 0.25, 0.5, 1, 2, 5, 8, 12, and 24 h postdose, and the plasma isolated after centrifugation was diluted and analyzed for parent compound by LC/MS-MS. (For compound **10**, the upper and lower limits of quantitation were 3.9 and 4000 ng/mL respectively.) These data were then used to calculate values for exposure, half-life, volume of distribution, clearance, and bioavailability .

Carrageeanan-Induced Paw Edema (CPE).[39] Groups (n = 5) of male Sprague−Dawley rats were dosed at t = 0 with **10** or pred followed by carrageenan injection into the rear footpad of the mouse at t = 2 h. At t = 5 h, the animals were euthanized, and the amputated hindpaws were weighed as a measure of overall anti-inflammatory activity. Paw exudate was extracted and evaluated for expression of IL-1β in response to the carrageenan stimulus by enzyme-linked immunosorbent assay (kit: rIL-1β: RLB00, R&D). Error bars represent the SEM of mean values for each dose group

Collagen-Induced Arthritis (CIA). CIA was assayed using published protocols.[41] Female Lewis rats were injected with collagen in the base of the tail, and disease was allowed to develop for 14 d. Groups (n = 10) of rats responding to the collagen challenge were selected and dosed daily with **10** or pred over the course of the following 15 d. Histology scores from Figure 2c were provided by BoulderBiopath (http://bolderbiopath.com/) after blinded samples from CIA study animals in all dose groups were sent for analysis. A p value of less than 0.01 by Students t test versus the untreated vehicle control group is deemed statistically significant. PK assessment was done at the end of study (day 15) following the rat PK protocol similar to that cited above except blood samples were collected via tail the vein of the Lewis rat.

Protein Expression, Purification, and Crystallization. Recombinant GR LBD (residues 522−777, F602Y, C638G) was expressed in *Escherichia coli* as a cleavable N-terminally his-tagged SMT-fusion and fermented in ZYP-5052 media in the presence of 0.05 mM C_1. A 250 mL amount of cells (BL21DE3 Codon Plus RIL, Stratagene) was grown in 2 L flasks at 37 °C for 3−5 h after a 20-fold dilution from a saturated culture after which the temperature was reduced to 22 °C to induce protein expression. The cells were harvested by centrifugation and then stored at −80 °C until processing. Cells were lysed by sonication in a buffer containing 0.02 M Tris pH 8.5, 0.5 M NaCl, 25 mM imidazole, 5 mM β-ME, 0.2 M NDSB-256, 0.2% β-octylglucoside, 10% glycerol, protease inhibitors (complete EDTA-free, Roche), and turbonuclease (Accelagen). Recombinant GR LBD was purified from the clarified cell lysate using Ni-NTA agarose (Qiagen) in batch mode. The Ni-NTA resin was collected in a drip column and washed with lysis buffer. Protein

was eluted with 0.02 M Tris pH 8.5, 0.5 M NaCl, 0.25 M imidazole, 5 mM β-ME and 10% glycerol. ULP1 protease (0.5%) was added to the eluted sample, and then, it was dialyzed overnight at 4 °C against 0.02 M Tris pH 8.0, 0.5 M NaCl, 10% glycerol, 0.2% β-octylglucoside, and 5 mM β-ME. The sample was reapplied to the Ni-NTA (His-TRAP HP, GE Healthcare), and the flowthrough was collected and concentrated for further purification by gel filtration (Sephadex 200, GE Healthcare) in 0.01 M Tris pH 8.5, 0.15 M NaCl, 0.2% β-octylglucoside, and 2 mM DTT. Before final concentration to 6 mg/mL, D30 peptide (HSSRLWELLMEAT) was added to a 3-fold molar excess relative to the protein, and **10** was added to one molar equivalent. The trimeric GR LBD/C_1/D30 complex crystallized in the space group $P2_12_12$ at 21 °C by vapor diffusion against 0.1 M bis-Tris pH 5.5, 0.3 M $Mg(COOH)_2$ using 1:1 drop ratio (0.3 μL). Crystals were cryoprotected using 25% ethylene glycol and cryocooled using liquid N_2.

Data Collection and Refinement. X-ray diffraction data were collected at the LRL-CAT beamline at the Advance Photon Source (Chicago, Illinois) (λ = 0.97931 Å). The data were processed using XDS. The crystal structure was determined by molecular replacement (one copy of the trimeric complex/au) using GR bound to dexamethasone as the search model (PHASER) and refined (BUSTER) at 2.35 Å resolution, after several rounds of model building (COOT), to an R_{work} of 17.9% and an R_{free} of 23.6% (Table 3). Residues 526−777 of GR LBD (chain A) are visible in the crystal structure except for a loop comprised by residues 703−710 for which representative electron density was lacking. Side chains for the following residues (chain A) are truncated due to incomplete electron density: K44, N759, and K777. Representative electron density is missing for residues 1, 12, and 13 of the D30 peptide (chain B) as well as for the side chain of R4. For C621 and L636, alternate side chain conformations are present. Unambiguous electron density was present for two copies of the ligand, one in the steroid binding site and a second in the crystal packing interface (Figure S3b, Supporting Information). There are 56 water molecules modeled into the structure. There are no residues in the disallowed region of the Ramachandran plot.

Table 3. X-ray Collection Data and Refinement Statistics

Crystal Parameters	
space group	$P2_12_12$
Cell Dimensions (Å)	
a	39.0
b	139.4
c	48.1
Angles (deg)	
α	90
β	90
γ	90
resolution (Å)	99−2.35
completeness (%)	99.9 (100)
R_{sym} (%)	10.6 (49.2)
mean $I/\sigma(I)$	13.9 (4)
redundancy	6.9 (6.8)
wavelength (Å)	0.97931
Refinement	
resolution range	2.35−25.36 (2.35−2.57)
reflections	11 492
R_{work}	17.9% (18.4%)
R_{free}	23.6% (24.0%)
rms dev. bonds	
lengths (Å)	0.01
angles (deg)	1.15
Total No. of Residues	
chain A	244
chain B	10
total no. protein atoms	2145
heteroatoms	118
ligand atoms	62
total no. waters	56
Average B (Å^2)	
peptide	
chain A	34.9
chain B	52.0
ligand	25.3
water	38.7

■ ASSOCIATED CONTENT

Supporting Information

Detailed in vitro comparisons of compound **10** versus reference standard steroids in binding and functional assays are shown in Table S1; PK data at the conclusion of the CIA live phase and normal Sprague−Dawley rats are summarized in Tables S2 and S3, respectively; additional information regarding the X-ray conformation of the **10**/GR LBD complex including electron density maps are provided in Figures S1−3; Figures S4 and S5 show crystal structures of dex and TFC in the GR LBD and of the mechanism of GR selectivity for **10**. This material is available free of charge via the Internet at http://pubs.acs.org.

Accession Codes

The coordinates for the structure of **10** within the GR LBD have been deposited in the Protein Data Bank under accession code 4LSJ.

■ AUTHOR INFORMATION

Corresponding Author

*Phone: (317) 651-1620; e-mail: coghlan_michael@lilly.com.

Present Address

§Chen Suen: chen.suen@nih.gov.

Author Contributions

M.J.C., J.L., C.S., and M.C. conceived and designed the experiments. D.T.K., T.M., N.S., B.C., M.M., D.C., and A.P. performed the experiments. A.E.S. collected human specimens. K.S.C., C.S.H., and J.P.H. analyzed the data. M.C., J.L., and M.J.C. wrote the paper. All authors have given approval to the final version of the manuscript.

Notes

The authors declare no competing financial interest.

■ ACKNOWLEDGMENTS

The authors gratefully acknowledge the staff at the LRL-CAT beamline at APS, Stephen Wasserman, Sonali Sojitra, John Koss, and Laura Morisco, for data collection. Use of the Advanced Photon Source at Argonne National Laboratory was supported by the U.S. Department of Energy, Office of Science, Office of Basic Energy Sciences, under contract no. DE-AC02-06CH11357. We are also indebted to V. Joe Klimkowski at Eli Lilly for the calculations of the binding volumes of the GR ligands and the activation energy between enantiomeric forms of **10**.

■ ABBREVIATIONS USED

GR, glucocorticoid receptor; GRE, glucocorticoid response element; MR, mineralocorticoid receptor; AR, androgen receptor; PR, progesterone receptor; ER, estrogen receptor; NHR, nuclear hormone receptor; TR, transrepression; TA, transactivation; dex, dexamethasone; pred, prednisolone; LBD,

ligand binding domain; TFC, trifluoromethylcarbinol; CPE, carrageenan induced paw edema; CIA, collagen induced arthritis; BPin, pinacol boronic ester

REFERENCES

(1) Steelman, S. L.; Hirschmann, R. Synthetic analogs of the adrenal cortical steroids. In *The Adrenal Cortex*; Eisenstein, A. B., Ed.; Little, Brown and Co.: Boston, MA, 1967; pp 345−383.

(2) Hirschmann, R. The cortisone era: Aspects of its impact. Some contributions of the Merck Laboratories. *Steroids* **1992**, *57*, 579−592.

(3) Hirschmann, R. Medicinal chemistry in the Golden Age of biology. Lessons from steroid and peptide research. *Angew. Chem., Int. Ed. Engl.* **1991**, *30*, 1278−1301.

(4) Coghlan, M. J.; Kort, M. E. Novel ligands of steroid hormone receptors. *Expert Opin. Ther. Pat.* **1999**, *9*, 1523−1536.

(5) De Bosscher, K. Selective glucocorticoid receptor modulators. *J. Steroid Biochem. Mol. Biol.* **2010**, *120*, 96−104.

(6) Newton, R.; Leigh, R.; Giembycz, M. A. Pharmacological strategies for improving the efficacy and a review. Therapeutic ratio of glucocorticoids in inflammatory lung diseases. *Pharmacol. Ther.* **2010**, *125*, 286−327.

(7) Labeur, M.; Holsboer, F. Molecular mechanisms of glucocorticoid receptor signaling. *Medicina* **2010**, *70*, 457−462.

(8) De Bosscher, K.; Beck, I. M.; Haegeman, G. Classic glucocorticoids versus non-steroidal glucocorticoid receptor modulators: Survival of the fittest regulator of the immune system? *Brain, Behav., Immun.* **2010**, *24*, 1035−1042.

(9) Berghe, W. V.; Francesconi, E.; De Bosscher, K.; Resche-Rigon, M.; Haegeman, G. Dissociated glucocorticoids with anti-inflammatory potential repress interleukin-6 gene expression by a NFκB-dependent mechanism. *Mol. Pharmacol.* **1999**, *56*, 797−806.

(10) Vanden Berghe, W.; Francesconi, E.; De Bosscher, K.; Resche-Rigon, M.; Haegeman, G. Dissociated glucocorticoids with anti-inflammatory potential repress interleukin-6 gene expression by a nuclear factor-κB-dependent mechanism. *Mol. Pharmacol.* **1999**, *56*, 797−806.

(11) Belvisi, M. G.; Wicks, S. L.; Battram, C. H.; Bottoms, S. E.; Redford, J. E.; Woodman, P.; Brown, T. J.; Webber, S. E.; Foster, M. L. Therapeutic benefit of a dissociated glucocorticoid and the relevance of in vitro separation of transrepression from transactivation activity. *J. Immunol.* **2001**, *166*, 1975−1982.

(12) Schacke, H.; Schottelius, A.; Docke, W.-D.; Strehlke, P.; Jaroch, S.; Schmees, N.; Rehwinkel, H.; Hennekes, H.; Asadullah, K. Dissociation of transactivation from transrepression by a selective glucocorticoid receptor agonist leads to separation of therapeutic effects from side effects. *Proc. Natl. Acad. Sci. U.S.A.* **2004**, *101*, 227−232.

(13) Clark, A. R.; Belvisi, M. G. Maps and legends: The quest for dissociated ligands of the glucocorticoid receptor. *Pharmacol. Ther.* **2012**, *134*, 54−67.

(14) Quax, R. A. M.; Peeters, R. P.; Feelders, R. A. Selective glucocorticoid receptor modulators: Future of glucocorticoid immunosuppressive therapy? *Endocrinology* **2011**, *152*, 2927−2929.

(15) Bledsoe, R. K.; Montana, V. G.; Stanley, T. B.; Delves, C. J.; Apolito, C. J.; McKee, D. D.; Consler, T. G.; Parks, D. J.; Stewart, E. L.; Willson, T. M.; Lambert, M. H.; Moore, J. T.; Pearce, K. H.; Xu, H. E. Crystal structure of the glucocorticoid receptor ligand binding domain reveals a novel mode of receptor dimerization and coactivator recognition. *Cell* **2002**, *110*, 93−105.

(16) Biggadike, K.; Bledsoe, R. K.; Coe, D. M.; Cooper, T. W. J.; House, D.; Iannone, M. A.; Macdonald, S. J. F.; Madauss, K. P.; McLay, I. M.; Shipley, T. J.; Taylor, S. J.; Tran, T. B.; Uings, I. J.; Weller, V.; Williams, S. P. Design and x-ray crystal structures of high-potency nonsteroidal glucocorticoid agonists exploiting a novel binding site on the receptor. *Proc. Natl. Acad. Sci. U.S.A.* **2009**, *106*, 18114−18119.

(17) Kauppi, B.; Jakob, C.; Farnegardh, M.; Yang, J.; Ahola, H.; Alarcon, M.; Calles, K.; Engstrom, O.; Harlan, J.; Muchmore, S.; Ramqvist, A.-K.; Thorell, S.; Ohman, L.; Greer, J.; Gustafsson, J.-A.; Carlstedt-Duke, J.; Carlquist, M. The three-dimensional structures of antagonistic and agonistic forms of the glucocorticoid receptor ligand-binding domain: RU-486 induces a transconformation that leads to active antagonism. *J. Biol. Chem.* **2003**, *278*, 22748−22754.

(18) Norman, P. Boehringer Ingleheim's selective glucocorticoid receptor agonist development candidate: Evaluation of WO2010141331, WO2010141332 and WO2010141333. *Expert Opin. Ther. Pat.* **2011**, *21*, 1137−1142.

(19) Norman, P. Crystalline forms of 2,2,2-trifluoro-N-[(1R,2S)-1-[1-(4-fluorophenyl)-1H-indazol-5-yl]oxy-1-(3-methoxyphenyl)-2-propanyl]acetamide (AZD-5423). *Expert Opin. Ther. Pat.* **2013**, *23*, 1239−1245.

(20) Madauss, K. P.; Bledsoe, R. K.; McLay, I.; Stewart, E. L.; Uings, I. J.; Weingarten, G.; Williams, S. P. The first X-ray crystal structure of the glucocorticoid receptor bound to a non-steroidal agonist. *Bioorg. Med. Chem. Lett.* **2008**, *18*, 6097−6099.

(21) Carson, M. W.; Coghlan, M. J. Preparation of a 6,11-dihydro-10-aza-dibenz[b,e]oxepin derivative as glucocorticoid receptor modulator. World patent application WO2008008882, 2008.

(22) Carson, M. W.; Coghlan, M. J. Preparation of (E)-N-[3-[1-(8-fluoro-11H-10-oxa-1-azadibenzo[a,d]cyclohepten-5-ylidene)propyl]-phenyl]methanesulfonamide as a glucocorticoid receptor modulator for the treatment of inflammatory and immune disorders. World patent application WO2009089312, 2009.

(23) Carson, M. W.; Giese, M. W.; Coghlan, M. J. An intra/intermolecular Suzuki sequence to benzopyridyloxepines containing geometrically pure exocyclic tetrasubstituted alkenes. *Org. Lett.* **2008**, *10*, 2701−2704.

(24) Uchida, H.; Mita, K.; Bekku, Y.; Nishimura, Y.; Ishida, Y.; Watanabe, K.; Tomikawa, S.; Inoue, S.; Sugimoto, H.; Nagao, T.; et al. Advantages of triple therapy with mizoribine, cyclosporine and prednisolone over other types of triple and/or double therapy including cyclosporine for renal transplantation. *J. Toxicol. Sci.* **1991**, *16*, 181−190.

(25) Uchida, K.; Era, T.; Nakasato, Y. Preparation of tetracyclic compounds as glucocorticoid receptor regulators. World patent application WO2011081173, 2011.

(26) Yu, H.; Richey, R. N.; Carson, M. W.; Coghlan, M. J. Cyclocarbopalladation of alkynes: A stereoselective method for preparing dibenzoxapine containing tetrasubstituted exocyclic alkenes. *Org. Lett.* **2006**, *8*, 1685−1688.

(27) Yu, H.; Richey, R. N.; Mendiola, J.; Adeva, M.; Somoza, C.; May, S. A.; Carson, M. W.; Coghlan, M. J. Stereoselective synthesis of dibenzoxapine containing tetrasubstituted exocyclic alkenes via cascade methylboronic acid coupling reactions. *Tetrahedron Lett.* **2008**, *49*, 1915−1918.

(28) Coghlan, M. J.; Green, J. E.; Grese, T. A.; Jadhav, P. K.; Matthews, D. P.; Steinberg, M. I.; Fales, K. R.; Bell, M. G. Preparation of derivatives of and analogs of dibenzosuberone for use in pharmaceutical compositions as steroid hormone nuclear receptor modulators. World patent application WO2004052847, 2004.

(29) Coghlan, M. J.; Jadhav, P. K.; Droste, J. J.; Green, J. E.; Matthews, D. P. Preparation of substituted tricyclic steroid hormone nuclear receptor modulators. World patent application WO2005066153, 2005.

(30) Gavardinas, K.; Green, J. E.; Jadhav, P. K.; Matthews, D. P. Preparation of tricyclic steroid hormone nuclear receptor modulators. World patent application WO2005066161, 2005.

(31) Labrosse, J.-R.; Poncet, C.; Lhoste, P.; Sinou, D. Asymmetric palladium(0)-mediated synthesis of 2-vinylchroman. *Tetrahedron: Asymmetry* **1999**, *10*, 1069−1078.

(32) Yardley, J. P.; Fletcher, H., III. Introduction of the methoxymethyl ether protecting group. *Synthesis* **1976**, 244.

(33) Huang, L.; Wong, P. K. Recent progress on the studies of the true catalyst in the Heck reaction with supported Pd particles. *Curr. Org. Synth.* **2010**, *7*, 599−613.

(34) Christen, D. P. Mitsunobu reaction. *Name React. Homol.* **2009**, 671−748.

(35) Putey, A.; Popowycz, F.; Do, Q.-T.; Bernard, P.; Talapatra, S. K.; Kozielski, F.; Galmarini, C. M.; Joseph, B. Indolobenzazepin-7-ones and 6-, 8-, and 9-membered ring derivatives as tubulin polymerization inhibitors: Synthesis and structure-activity relationship studies. *J. Med. Chem.* **2009**, *52*, 5916−5925.
(36) Coghlan, M. J.; Jacobson, P. B.; Lane, B.; Nakane, M.; Lin Chun, W.; Elmore, S. W.; Kym, P. R.; Luly, J. R.; Carter, G. W.; Turner, R.; Tyree, C. M.; Hu, J.; Elgort, M.; Rosen, J.; Miner, J. N. A novel antiinflammatory maintains glucocorticoid efficacy with reduced side effects. *Mol. Endocrinol.* **2003**, *17*, 860−869.
(37) Smith, C. J.; Ali, A.; Balkovec, J. M.; Graham, D. W.; Hammond, M. L.; Patel, G. F.; Rouen, G. P.; Smith, S. K.; Tata, J. R.; Einstein, M.; Ge, L.; Harris, G. S.; Kelly, T. M.; Mazur, P.; Thompson, C. M.; Wang, C. F.; Williamson Joanne, M.; Miller, D. K.; Pandit, S.; Santoro, J. C.; Sitlani, A.; Yamin, T.-t. D.; O'Neill, E. A.; Zaller, D. M.; Carballo-Jane, E.; Forrest, M. J.; Luell, S. Novel ketal ligands for the glucocorticoid receptor: in vitro and in vivo activity. *Bioorg. Med. Chem. Lett.* **2005**, *15*, 2926−2931.
(38) Zhang, J.-Z.; Cavet, M. E.; VanDerMeid, K. R.; Salvador-Silva, M.; Lopez, F. J.; Ward, K. W. BOL-303242-X, a novel selective glucocorticoid receptor agonist, with full anti-inflammatory properties in human ocular cells. *Mol. Vision* **2009**, *15*, 2606−2616.
(39) Morris, C. J. Carrageenan-induced paw edema in the rat and mouse. *Methods Mol. Biol.* **2003**, *225*, 115−121.
(40) Van Den Berg, W. B.; Joosten, L. A. B. Murine collagen-induced arthritis. In *In Vivo Models of Inflammation*; Morgan, D. W., Marshall, L. A., Eds.; Birkhauser Verlag: Basel, Switzerland, 1999; pp 51−75.
(41) Bendele, A.; Mccomb, J.; Gould, T.; Mcabee, T.; Sennello, G.; Chlipala, E.; Guy, M. Animal models of arthritis: Relevance to human disease. *Toxicol. Pathol.* **1999**, *27*, 134−142.
(42) Biggadike, K.; Bledsoe, R. K.; Hassell, A. M.; Kirk, B. E.; McLay, I. M.; Shewchuk, L. M.; Stewart, E. L. X-ray crystal structure of the novel enhanced-affinity glucocorticoid agonist fluticasone furoate in the glucocorticoid receptor-ligand binding domain. *J. Med. Chem.* **2008**, *51*, 3349−3352.
(43) Schoch, G. A.; D'Arcy, B.; Stihle, M.; Burger, D.; Bar, D.; Benz, J.; Thoma, R.; Ruf, A. Molecular switch in the glucocorticoid receptor: Active and passive antagonist conformations. *J. Mol. Biol.* **2010**, *395*, 568−577.
(44) Brzozowski, A. M.; Pike, A. C. W.; Dauter, Z.; Hubbard, R. E.; Bonn, T.; Engstrom, O.; Ohman, L.; Greene, G. L.; Gustafsson, J.-A.; Carlquist, M. Molecular basis of agonism and antagonism in the estrogen receptor. *Nature* **1997**, *389*, 753−758.
(45) Suino-Powell, K.; Xu, Y.; Zhang, C.; Tao, Y.-g.; Tolbert, W. D.; Simons, S. S., Jr.; Xu, H. E. Doubling the size of the glucocorticoid receptor ligand binding pocket by deacylcortivazol. *Mol. Cell. Biol.* **2008**, *28*, 1915−1923.
(46) A second copy of **10** found at the crystal packing interface is not deemed biologically relevant.